-RESEARCH PAPER-

International Journal of Mining and Geo-Engineering

IJMGE

IJMGE 59-1 (2025) 51-60

DOI: 10.22059/IJMGE.2025.360584.595075

Experimental study on the cyclic swelling- shrinkage behavior of soil in the Algerian region of N'Gaous

Benabdelmoumene Zakaria [a,*], Mohamed Baheddi [b] and Imene Bougouffa [b]

[a] *Laboratory of Natural Risk and Regional Planning (LRNAT), Department of Civil Engineering, Faculty of Technology, University of Batna 2. Batna, Algeria.*

[b] *Department of structures and materials, Faculty of Civil Engineering, University of Houari Boumediene USTHB, Algeirs, Algeria.*

Article History:

Received: 10 June 2023.

Revised: 04 December 2024.

Accepted: 18 February 2025.

ABSTRACT

The phenomenon of swelling-shrinkage has gained widespread attention in practice owing to the generation of eroded clayey layers of soil that amplify with global climate change and the seasonal water content. This provokes several serious disorders affecting the stability of nearby constructions and consequently generating human loss. The expansive clayey soils show the phenomena of wetting and drying cycles in their natural state (undisturbed soil). Hence, classical oedometric tests are found to be unable to take into account the thermal behavior of naturally swelling soils; this is proven by the resulting asymptotic volumetric behavior, as well as the steady values of the potential of swelling and shrinkage. The main aim of this experimental analysis is to derive a test that considers the significant effect of temperature. Experimental results of an oedometric approach are represented herein for the purpose of investigating the volumetric and hydric behavior of naturally swelling soil in the region of N'Gaous (Eastern Batna province, Algeria) through drying-wetting paths. Innovative expressions are derived for the direct computations of the swelling-shrinkage potential in terms of water content, appearance time and applied loads. It is of interest to mention that those expressions are applicable to other regions in the world with similar soil geotechnical and chemical characteristics and conditions. The cyclic outputs show that the swelling pressure variation with the appearance time is mainly related to the first cycle of swelling-shrinkage; as it exhibits a noticeable increase in the swelling potential with the amplification of applied loads until reaching a state of steadiness. The experimental results demonstrate a high degree of reliability and correlation with the soil behavior. Therefore, the swelling-shrinkage potentials are expressed innovatively in equations that help predict the soil behavior in expansive regions in order to enhance the safety of nearby foundations.

Keywords: *Clayey soil, Infiltration velocity, Swelling-shrinkage phenomena, Swelling pressure, Wetting-drying paths.*

1. Introduction

The swelling-shrinkage is a global phenomenon that has been known for decades in clayey soils; it appears notably in tunnels or road and underground infrastructures. In addition, several serious disorders might induce the instability of nearby foundations and consequently generate human loss. The relevant economic issues are estimated at millions or even billions of Euros, in which several regions in Algeria have undergone this drawback, namely, Boumagueur, Medea, Tlemcen, and Batna [1–6]. The prevailing type of soil that dominates in those arid or semi-arid zones is that of the unsaturated type [2,7,8]. These studies conducted analyses on disturbed soil samples, without accounting for the alterations in the initial mechanical and physical characteristics. This may trigger changes in the microstructure of the considered soil in the above-mentioned regions as proven by Rathore and Tiwari [9], Rao et al. [10], and Nabil et al. [11]. This is explained by the generation of uneven stress distribution that leads to the localization of swelling and shrinkage, affecting the boundary conditions, in which the hydraulic conductivity and the capillarity will prolong the duration of the process to reach ultimate values of swelling and shrinkage.

It should be emphasized that the soil volumetric behavior varies with respect to water absorption. This is interpreted by the fact that in the case of wetting, the pertinent soil characteristics are derived by means of the increase in the soil volume, degree of saturation, Atterberg limits, natural water content, potentials of swelling and shrinkage, and swelling pressure; as well as the chemical composition [12]; and vice versa for the case relevant to dryness. Clayey soils are composed of various minerals (kaolinite, smectite, illite and montmorillonite) that have power to vary the swelling magnitude due to their composition affecting the volume of soil [5]. The permeability of montmorillonite in particular is considered to be quite aggressive toward swelling [2]. In terms of the mineralogical and granulometric characteristics of soil, the capillary and film absorption types are the ones that dominate, whereas the film absorption in particular follows constantly a swelling trend. The results obtained from Djedid et al. [13] exhibit lower heave and increased shrinkage analogous to the increase in the number of cycles. This refers to the amplified formation of cracks within the soil, causing permanent volume variations.

In this critical context, the study of this phenomenon has to be extremely broadened in order to encompass all disorders related to its appearance and evolution. Basically, in the geotechnical or construction fields, the core reason for this foundation soil disorder is directly related to its swelling-shrinkage cycles in rainy or dry seasons (wetting-drying paths)[14–16]. It was deduced from Soltani et al. [17] that thermal

* Corresponding author. *E-mail address:* z.benabdelmoumene@univ-batna2.dz (B. Zakaria).

fluctuations on distributed soils exhibit the development of air pockets that vary heat transmission, influencing the hydraulic and the volume of expansive soils. Hence, the results obtained from Abbas et al. [18] for remodeled samples show that the stress boundary and wetting conditions are the main controlling factors of the expansive soil response to thermal alterations. Mustafaev [19] has found that the mechanism of structural deformation in expansive soils is mainly due to the intracrystalline swelling in the mineral particles, as well as the interaction of water content with the interparticle cohesion. The absorption of soil was taken into account with respect to matrix and osmotic magnitudes. This matrix magnitude is the negative pressure that maintains the pore pressure in equilibrium by means of a porous membrane. It was deduced that the suction force determines the rate of permeability pertaining to clayey soils, which affects the incidence of swelling. Huang et al. [14] exhibit the significant influence of dry density and vertical stress on the pressure and swelling deformation.

The investigation of the soil cyclic impact on the overall stability, including the durability of infrastructures was addressed by Khennouf and Baheddi [7] and Zemenu et al. [20]. The studies focused on the foundation design, while considering the embedment length and stiffness. Onyelowe et al. [21] applied artificial techniques in order to address soil stabilization; it was found that hybrid sawdust ash (HSDA) has proven its effectiveness as a substitute for classic Portland cement. Also, Onyelowe et al. [22] employed artificial intelligence (AI) to address the soil stabilization method based on pressing criteria for carbon emissions. It was noted from the study conducted by Dao [23] that the number of wetting-drying cycles leads to an extended rate of cracks, as the length and surface area were amplified noticeably. It should be noted that AI has shown precision refinement of the estimation of swelling and shrinkage stresses, while addressing boundary conditions affecting soil stabilization [24,25]. Aneke et al. [26] investigated the effectiveness of two approaches that rely on the artificial neural network, namely general regression and backpropagation. Those predictive models proved to be accurate in the assessment of swelling stress.

The present paper extends those studies to investigate the effect of intact soil under thermal conditions, with due regard to the standard test methods [27–30]. The classical oedometric tests are quite limited for the determination of swelling soil behavior during seasonal fluctuations. The latter may cause significant variations in soil volume, especially in tropical climates; given that the moisture in clays may evaporate remarkably under relatively higher temperatures.

Puppala [31] showed that the moisture content of soil influences significantly the compaction behavior, as well as the swelling and shrinkage characteristics of high plastic soils in different sites. In this paper, the oedometric test is modified in order to adjust to the innovative thermal variable that influences significantly the cyclic evolution; as well as the potential of swelling- shrinkage. The soil microstructure is saved from alterations by preserving the physical and chemical properties of the extracted specimens (intact specimens), while maintaining similar thermal conditions to the region of N'Gaous (Batna province, Algeria). The cyclic analysis of the water content is investigated in terms of time under each loading; as well as the effect of time and water content on the potentials of swelling and shrinkage. Hence, new expressions are derived for the computation of cyclic evolutions.

2. The case study

2.1. Geological description

The geological maps in Figure (1) indicate that the case study is located in the Algerian region of N'Gaous, precisely in the eastern side of Batna city.

Extraction points are performed in zones 1-4, as shown in Tables (1 and 2), which signify 90% of pathologic similarities. Table (3) recapitulates the physico-mechanical characteristics of the extraction zones, from which the Atterberg limit is computed, in order to depict the plastic behavior. Figure (2) shows that the plasticity index computed in terms of liquid limit pertaining to zone 1 is greater than the other zones, indicating more significant volumetric changes. Therefore, the characteristic study is conducted for the most affected site (zone 1) by degradations caused by swelling-shrinkage phenomena, as indicated in Figure (3). It should be mentioned that this zone is occupied by a four-story construction near a hospital (Figure (1)).

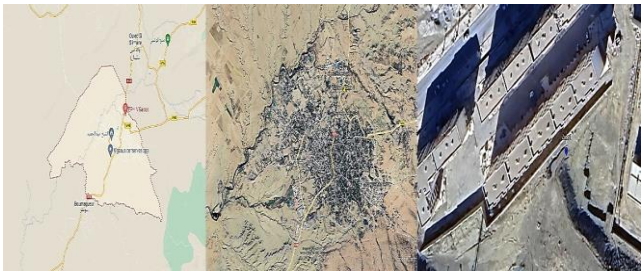

Figure 1. Case study of the region N'Gaous (Batna, Algeria).

Table 1. Geological description of zone 1 pertaining to the four floor construction.

Zone 1	Description
Location	Lat.35.56801325°, Log.5,61644055°
Depths	**Lithology**
0.0 à 0.50 m	Clayey topsoil
0.50-1.50 m	Clayey sand, Compact greenish marl, with a little traces of carbonate
1.50-8.00 m	Greenish marl, with carbonate traces

Table 2. Geological description of zones 2,3, and 4 pertaining to 50 lodgings.

Zones 2-4	Description
Location	Lat.35.545968°, Log.5,604202823° Lat. 35.331504°, Log 5.363026° Lat. 35.325547°, Log 5.364120
Depths	**Lithology**
0,0-0,60 m	Clayey topsoil
0,6-1.00 m	Sandy Clay with traces of gypsum (explosion of the specimen)
1,20-8,00 m	Greenish marl with traces of carbonate

Table 3. Comparison of different physico-mechanical characteristics pertaining to extraction zones.

Depth	2,80-4,40m			
	Zone 1	Zone 2	Zone 3	Zone 4
Cohesion C (bars)	0,9	0,66	0,37	0,85
Friction angle φ (°)	18	22,56	24,56	20,98
Water content w (%)	13,06	16,16	16,42	19
Plasticity index I_P (%)	43,07	34,48	25,61	16,78
Liquid limit W_L (%)	72,58	63,48	55,28	46,38
Plastic limit W_P (%)	29,51	29	29,66	29,6
Void ratio e	0,45	0,54	0,53	0,52

2.2. Chemical and mineralogical composition of the studied soil

The response of expansive soils to moisture is primarily controlled by the type and percentage of mineral content. These index properties are essential for evaluating the swelling pressure of clayey soils, as they are significantly influenced by the microstructural characteristics, and exchangeable ions. Understanding these factors is vital for civil engineering applications, particularly in foundation design and soil stabilization. The chemical, mineralogical and X-ray diffraction (XRD) analyses shown in Tables (4 and 5) and Figure (4) are added in the

framework of this research for the purpose of obtaining a complete identification of the soil. The Unified Soil Classification System USCS/LCPC classifies the soil from the region of N'Gaous as clay of a high degree of plasticity CH with low organic matter. The X-ray fluorescence (XRF) analysis presented in Table 4 reveals a significant silica content of approximately 49.53%, while alumina makes up 17.97%. These two chemical constituents are the primary components of clay minerals, playing a critical role in determining the physical and engineering properties of the soil. Figure (4) shows the mineralogical composition of the analyzed soil, characterized using XRD techniques. The soil is comprised of 18.5% quartz and 69.7% clay minerals. This includes 47% montmorillonite, 6.7% illite, and 16% kaolinite. This composition is crucial for understanding the soil's physical and chemical behavior. The present study is focusing on undisturbed (intact) specimens, extracted from zone 1 at a depth of 2.80-4.40m, since this zone is recognized as the most unfavorable area (critical). Hence, a comprehensive overview of the physical and mechanical characteristics is provided in Table (6).

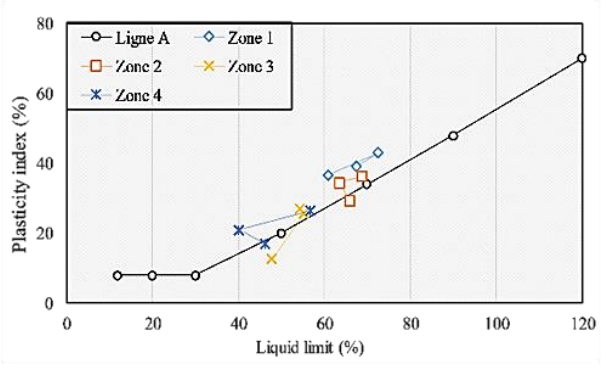

Figure 2. Casagrande diagram for different zones.

Figure 3. The generated cracks in zone 1.

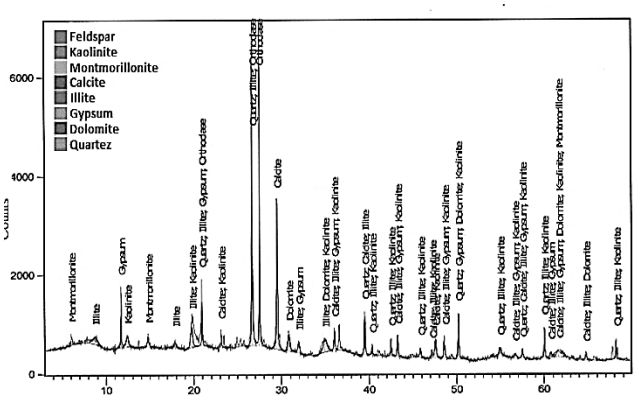

Figure 4. XRD relevant to zone 1

Table 5. Chemical properties of the soil pertaining to zone 1.

Denomination	Na^+K	Ca^{++}	Mg^+	Cl^-	SO_4	HcO_3	Co_3	Ph
Unite %	13.05	1.51	0.45	0.02	6.65	0.92	0.5	7.9

Table 6. Physico-mechanical characteristics pertaining to zone 1.

Characteristics of soil	Symbol	Unite	Values
Depth		2.80-4.40 m	
Water content	w	%	13.06
Degree of saturation	S_r	%	78.9
Dry unit weight	γ_d	kN/m³	18.3
Wet unit weight	γ_h	kN/m³	20
Solid unit weight	γ_s	kN/m³	26.5
Void ratio	e	/	0.45
Porosity	n	/	0.31
Liquid limit	W_L	%	72.58
Plastic limit	W_P	%	29.51
Plasticity index	I_p	%	43.07
Cohesion	C	bars	0.90
Friction angle	φ	°	18
Deformation modulus	E	MPa	12.1
Value of methylene blue	VB_s	g/100g	7.8
Percentage of clay	A_C		0.57
Caco3		%	41
Content of organic matter		%	7.8
Granulometry			
Sand	/	%	3.8
Silt	/	%	20.3
Clay	/	%	75.9
C80 μm		%	98.5
C2 mm		%	69.7

3. Experimental approach

It is known that the classical oedometric tests following the norms of ASTMD-4546-03 (American Society for Testing and Materials) [28], ASTMD-4546-03[29] and XP P 94-090-1[30] are quite limited for the consideration of the thermal factor during cyclic computations of swelling-shrinkage. Therefore, the elaboration of a similar test with the condition of taking into account this functionality has become a necessity in this paper. Subsequently, the used oedometric cell is attached to a heating resistor at the base, and covered with an insulating wall and impervious lid, as shown in Figure (5).

The extracted specimens are undisturbed marl clay, which have been paraffined for reasons to avoid the distortion of natural characteristics during transport towards the National Laboratory of Habitat and Construction LNHC-Batna. Twenty specimens are prepared in the laboratory by replicating the environmental conditions for the precision in the estimation of the soil characteristics recapitulated in Table (6). The sample is subsequently placed in a conventional oedometer cell and saturated with water while incremental loads P are applied, ranging from 0 to 3 bars.

Table 4. Chemical properties of the mineral soil pertaining to zone 1.

Silica	Alumina	Sodium	Calcium	Magnesium	Potassium	Ferric Oxide	Sulfur	chlorine	Titan Dioxide	Manganese dioxide
SiO2	Al_2O_3	Na_2O	CaO	MgO	K_2O	Fe_2O_3	SO_3	Cl	$TiO3$	MnO_2
49.53	17.79	0.70	6.9	2.52	2.17	6.65	0.2	0.02	0.82	0.11

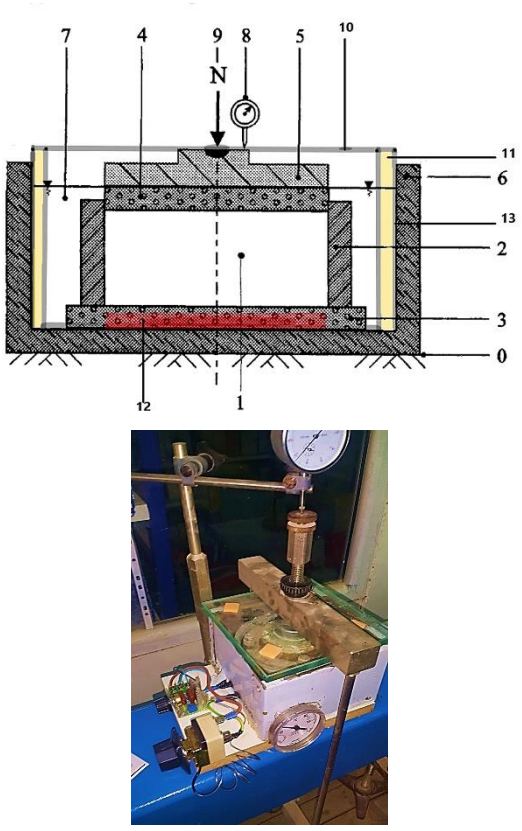

Figure 5. Prototype relevant to the modified oedometric equipment, with: 0) Frame cell, 1) Material specimen, 2) oedometric ring, 3) bottom porous stone, 4) Top porous stone, 5) Pressure pad, 6) Reservoir, 7) Imbibition liquid, 8) Dial gauge, 9) Loading yoke, 10) Heat-tempered glass with drainage tube, 11) Thermal insulator, 12) Electrical heating resistor with temperature regulator, and 13) Austenitic stainless steel plate.

This procedure induces vertical deformations, which are measured using a dial gauge (Figure (6)) according to the duration of load application. Once steady deformations are reached at an atmospheric temperature, a desiccating stage should begin gradually to replicate the regular behavior of the soil. Beyond the occurrence of a full swelling and contraction of the specimens (acquisition of stable heights), the saturation phase takes place for the subsequent cycle. Hence, a series of wetting and drying cycles are depicted until equilibrium. A comprehensive overview of the oedometric characteristics is provided in Tables (7).

Figure 6. Oedometric frames with modified cell support and resistance (LNHC-Batna).

Furthermore, the velocity of water infiltration V is illustrated in Figure (7), showing the evolution of water absorption by the soil within the humidification period, with respect to loading magnitude pertaining to the first cycle. The infiltration velocity is influenced by the soil granulometric properties. In the initial phase, the velocity is seen to be dropping progressively with a constant range of 10% from the case of P=0 to the rest of cases at t= 1day; beyond which, the percentage decreases to 4% at 7 days. As time elapses the plots tend to converge towards lower velocity ranges until approaching a null point.

Table 7. Oedometric properties of the soil pertaining to zone 1.

Parametres	Symbols	Values
Swelling pressure	P_g(kPa)	690
Preconsolidation pressure	P_c(kPa)	750
Oedometric modulus	E_{oed}(MPa)	16.29
Compression index	C_c	0.55
Swelling index	C_s	0.046
Coefficient of compressibility	a_v(1/MPa)	0.091
Poisson's ratio	v	0.3
Volumetric modulus	K(MPa)	10.08
Shear modulus	G(MPa)	4.65
Coefficient of permeability	K_v(m/s)	$2.8x10^{-10}$

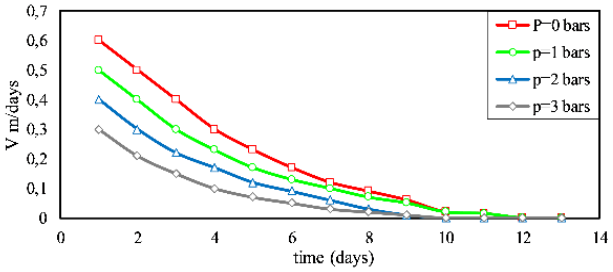

Figure 7. Infiltration velocity in the soil sample relevant to zone 1.

4. Interpretation of the results

The impact of temperature on the swelling process at the free state (no loads are applied) is investigated for a range of 20°C (natural atmospheric temperature of the laboratory) and 35°C. Figure (8) indicates that at 35°C, the swelling strain (zone 1) is enhanced by 22% compared to T=20°C. This gap shouldn't be passed over in the assessment of soil suitability for building. Subsequently, Figure (9) points out the impact of T=35°C that is remarkably depicted in zone 1. This shows amplified plots compared to other zones in the considered area. For this reason, this temperature (35°) is adopted to conduct all analyses in this paper, in order to preserve the microstructure and boundary conditions, preventing the localization of swelling and shrinkage within the soil.

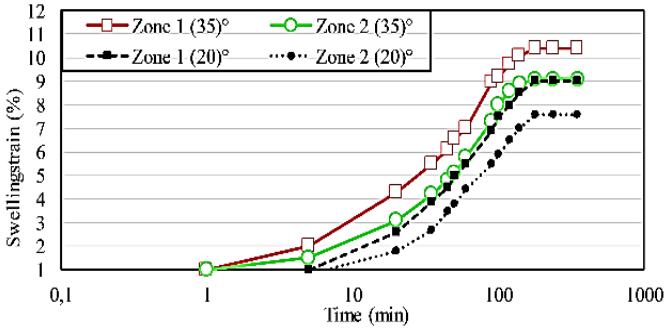

Figure 8. Effect of temperature on the development of swelling strain with time progression in the free state.

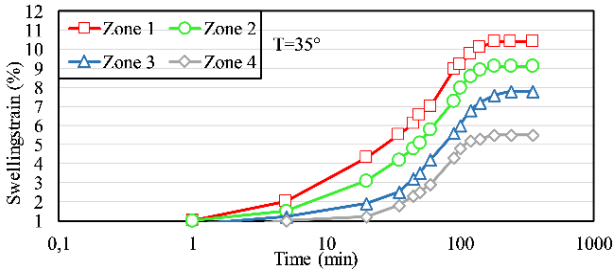

Figure 9. Free swelling strain versus time, under the critical temperature T=35°.

Figure (10) illustrates a comparison between the current study and that of Huang [14], Mustafaev [19] and Puppala [31]. This research investigated the response of soil under several conditions throughout compaction; explicitly, drier soil than the optimum moisture content (Dry of OMC), soil at maximum dry density (OMC), and wetter soil than the optimum moisture content (Wet of OMC). It is seen that the compaction rate of soil is reduced for lesser lubricant soil particles, which results in more pronounced swell strains. The plots of all studies are following an increasing trend with the increase of the heave $\mathcal{E}_{Sw}$ and time t, by dint of the expanded contact between soil particles and water at a temperature fluctuating between 20° to 35°C. The reached steady values refer to the ultimate aptitude of volume alterations; this is endorsed by the full saturation of voids. The curves tendency of the current study is aligned with the findings of previous studies. However, the slight difference between plots to reach stable values is controlled by the water content factor of each considered soil.

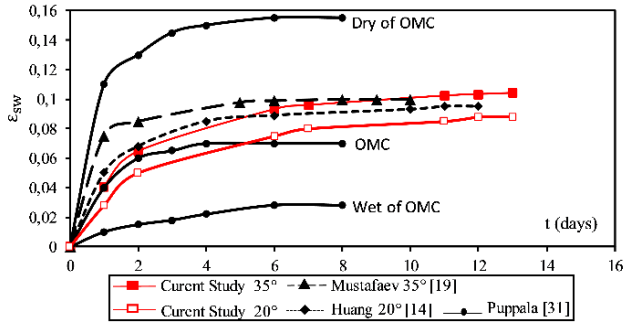

Figure 10. Comparison between the current study and earlier studies.

4.1. Cyclic analysis for the water conten under the action of various loads

Wetting and drying cyclic tests are implemented herein by means of the improved oedometer; axial displacements are depicted progressively until attaining irreversible variations. Heave-contraction plots are engendered for various ranges of surcharge pressure P= 0 to 3 bars, and time (t). The swelling-shrinkage potentials are dressed with a curve representing the deformation in terms of water content. Figure (11) shows the cyclic evolution of the water content w (%) in terms of time t (days). The variation of soil volume increases significantly that pertaining to the initial soil moisture. The stabilization of the swelling deformation occurs for a considerable elapsed time with respect to the infiltration of water; contrasting with the shrinkage deformation. The maximum saturation generated for the initial cycles of wetting is as great as 30%, reached at t=0 to 13 days. Thereafter, the mean value relevant to shrinkage w=7% is obtained at t= 13 to 26 days. Figure (11) indicates that for P=0 to 3 bars, the 1st cycle undergoes diminutions in the water content of swilling w_{Sw} that are from 6.83% to 10.38%, while it is of 8,82% to 11,12% and from 10,28% to 12,78%, respectively for the 2nd and 3rd cycles. The water content of shrinkage w_{Shr} drops from 0.29% to 3.40% for the 1st cycle, and it is in the interval of 0- 0.71% for the 2nd and 3rd wetting cycles. While for the drying case, all three cycles result in a quite tight band in terms of water content, independently of the loading, as shown in Table (8). In physical terms, the decreasing tendency in the water content with the cyclic variations is due to the change in density of the pores relevant to the solid particles. It is noted that during the process of swelling, the rise in the intensity of external loadings leads the water absorption to drop noticeably. It should be mentioned that this volumetric variation is not applicable to the shrinkage. During the loading increase, the diminution of the soil porosity coefficient leads to the absorption capacity to drop.

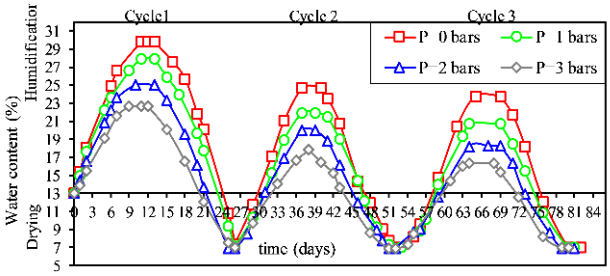

Figure 11. Cyclic variation of w (%) with time t (days).

Table 8. Cyclic evolution of the water content w (%) under loading P (bars).

Loads (bars)	Cycle 1		Cycle 2		Cycle 3	
	w_{Sw}%	w_{Shr}%	w_{Sw}%	w_{Shr}%	w_{Sw}%	w_{Shr}%
P=0	30	7,35	24.69	7.03	24	7
P=1	28	7,10	22	7	21	7
P=2	25,50	7	20.06	6,95	18,30	6,95
P=3	22,50	6,98	17.83	6,94	16,41	6,95

4.2. Mathematical model for wetting-drying paths by means of water content

New expressions are derived respectively for the cycles pertaining to swelling (Eq. (1)) and shrinkage (Eq. (2)), in order to permit a mathematical approach to interpret the deformations that the soil is undergoing during wetting-drying paths. These expressions are applicable for all studies involving periodic processes, regarding the complex dynamics of expansive soil response in the long term, assimilating both persistent aspects and periodic alterations.

$$w_{Sw}(t) = a\,sin\big(b(t+c)\big) \quad (1)$$

$$w_{Shr}(t) = a\,sin\big(b(t-c)\big) \quad (2)$$

Where, a, b, c and k are coefficients in terms of $w(t)$ and P. Table (9) recapitulates all possible values necessary for the dressing of curves in Figure (12). Mustafaev [19] has developed another expression of w(t) using the method of Fourier (Eq. (3)), as shown in Figure (13).

Table 9. Magnitude of the coefficients a, b, c and k employed in Eqs. 1 and 2.

Coefficients	Cycle 1	Cycle 2-3
a	-10,534+121,24/(P+3,331)	-18,27+507,68/(P+18,62)
b	2,76-274,71/(P+103,338)	0,23-0,014/(P+1,61)
c	-4,47+15,54/(P+1,926)	-3,29-0,19/(P-0,51)
k	17,68-11,69/(P+0,85)	-10,06+428,8/(P+16,44)

Mustafaev [19] takes into consideration the variables A and B, as well as the water content pertaining to both swelling and shrinkage, so that the sum of quadratic deviations pertaining to the given function in terms of $w(t)$ values of respective arrangements becomes the minimum. Under those conditions, a linear equation system is obtained according to the theory of Fourier leading to the general relationship in Eq. (3). This function is derived with respect to the conditions of Dirichlet; whereas t is in the interval of 0 to 2π:

$$w(t) = A_0 + \sum_{i=1}^{n}(A_i \cos it + B_i \sin it) \quad (3)$$

$$A_0 = \frac{1}{2\pi}\int_0^{2\pi} w(t)dt \quad (4)$$

$$A_i = \frac{1}{\pi}\int_0^{2\pi} w(t)\cos it\,dt \quad (5)$$

$$B_i = \frac{1}{\pi}\int_0^{2\pi} w(t)\sin it\,dt \quad (6)$$

It is found from Figure (14) that Eq. (3) derived with respect to Eqs. (4-6) in order to determine the water content evolution during the test has shown an excellent agreement with the current results relevant to Eqs. 1 and 2 that are developed to consider the loading in the computation of swelling-shrinkage.

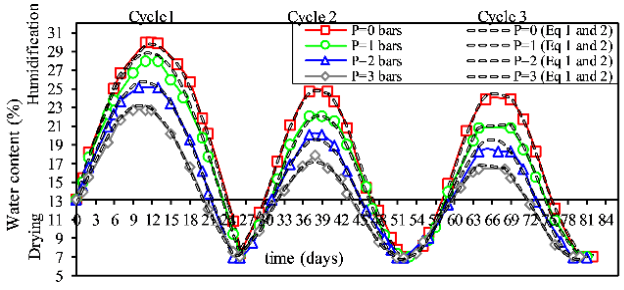

Figure 12. Application of the derived equations relevant to cyclic variations of w (%).

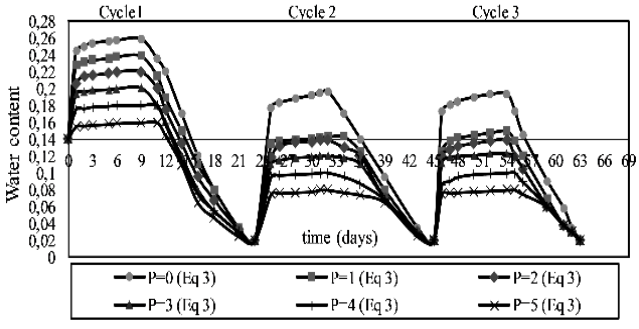

Figure 13. Cyclic variation of water content dressed using Eq. 3 of Mustafaev [19].

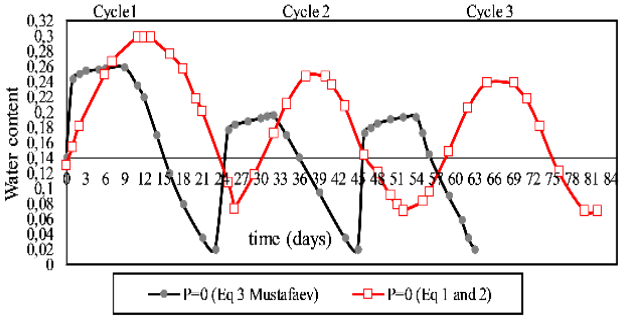

Figure 14. Correlation between Eqs.1 and 2 from the current study and Eq. 3 of Mustafaev [19].

4.3. Factors influencing cyclic evolutions of the swelling and shrinkage strains

4.3.1. The effect of time

The potentials of swelling $\mathcal{E}_{Sw}$ and shrinkage $\mathcal{E}_{Shr}$ are determined with respect to the variation in the water content relevant to the wetting-drying paths; this is fulfilled through the use of the prototype pertaining to the modified oedometric test that permits the control of cyclic variations relevant to the water content. Figures (15 and 16) represent a comparison between the behavior of the expansive soil extracted from the region of N'gaous and that affected by the Caspian Sea in Azerbaijan studied by Mustafaev [19]. Both figures show the variation of swelling and shrinkage potentials with time for P varying from 0 to 3 bars. The present study is in good agreement with the earlier one; both studies resulted in a discernible parallelism, as the time escalates, both $\mathcal{E}_{Sw}$ and $\mathcal{E}_{Shr}$ exhibit a relevant increase in a steady manner until reaching constant values subsequent to an extended time interval. However, the discrepancy between the curves refers to the fact that the present study emphasizes the effect of initial water content and dry density while not addressing the chemical and mineralogical compositions of all existing expansive soils, notably the type of clay accounted for by Mustafaev. In addition, the environmental and moisture fluctuations with the seasonal changes may affect significantly the results, as indicated above in Figures 10 and 11, showing that the cyclic variation has an impact on the magnitude of swelling-shrinkage under different loadings. It is noted from both Figures 15 and 16 that the shrinkage plots obtained from Mustafaev are more conservative and distinguishable under the effect of loads compared to the present study, due to the fact that the soil near the coastal area studied by Mustafaev can uphold more steady water balance (rarer fluctuations in the humidity originating from the Caspian Sea). The climate variation from the arid/semi-arid climate (drier and less humid) of north Africa to the stable climate of Azerbaijan leads to more pronounced shrink cycles and conservative responses to applied loadings in the African region (present study), by dint of the rise in drought and rain cycles. The experimental results are recapitulated in Table (10); it is noted that the outcomes pertaining to all cycles are aligning with the same overarching path. This stems from the increase in P that leads $\mathcal{E}_{Sw}$ to drop and $\mathcal{E}_{Shr}$ to rise; in which it refers to the effect of loads on the water absorption through soil pores. The upward trajectory of expansive-contraction cycles results in slight increases in the corresponding potentials; which means, the soil particles are undergoing significant deformations that may lead to a deficiency in the design of nearby foundations.

4.3.2. The effect of water content

Figure (17) depicts the effect of water content on the soil behavior in a long-term time scope; the curves are interpreted in Table (11). It is deduced from the alterations in $\mathcal{E}_{Sw}$ and $\mathcal{E}_{Shr}$ with respect to each loading that the clay is deforming, due to the lack of sustainability generated from its composition and geo-topographic site. For P=0 bars, $\mathcal{E}_{Sw}$ rises in value from 0 to 1.93% (1st-3rd cycles), and $\mathcal{E}_{Shr}$ from 0,1 to 0,49%. P=1 bars results in $\mathcal{E}_{Sw}$ as great as 0.25%, and $\mathcal{E}_{Shr}$ of 0.4-1.49%. P=2 bars increases $\mathcal{E}_{Sw}$ from 3.04 to 5%, and $\mathcal{E}_{Shr}$ from 0.76 to 2.01%. Hence, P=3 bars shows a rise in $\mathcal{E}_{Sw}$ from 1.58 to 2.33%, and in $\mathcal{E}_{Shr}$ from 1 to 1.64%.

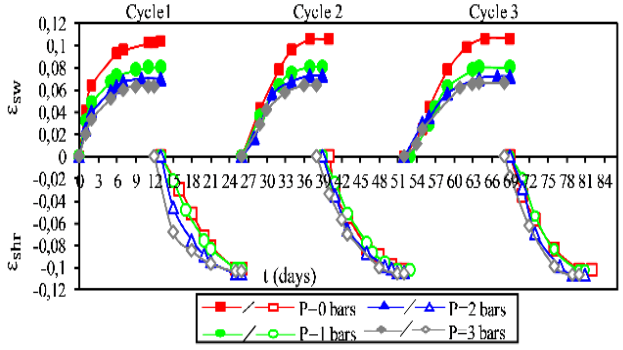

Figure 15. Cyclic variation of the swelling-shrinkage potentials in terms of t and P.

Table 10. Application domain of the evolutionary swelling-shrinkage potentials in terms of different cyclic loadings.

Loads (bars)	Cycle 1		Cycle 2		Cycle 3	
	$\mathcal{E}_{Sw}$	$\mathcal{E}_{Shr}$	$\mathcal{E}_{Sw}$	$\mathcal{E}_{Shr}$	$\mathcal{E}_{Sw}$	$\mathcal{E}_{Shr}$
P=0	0.1035	-0.1015	0.1055	-0.102	0.1065	-0.1021
P=1	0.0807	-0.101	0.0805	-0.1025	0.0805	-0.1024
P=2	0.07	-0.1051	0.0735	-0.1043	0.072	-0.1064
P=3	0.0635	-0.1034	0.0645	-0.1053	0.066	-0.1065

Table 11. Results of the cyclic variation of the swelling-shrinkage potentials in terms of water content w.

	Cycle 1				Cycle 2				Cycle 3			
Loads (bars)	ε_{Sw}	w_{Sw} (%)	ε_{Shr}	w_{Shr} (%)	ε_{Sw}	w_{Sw} (%)	ε_{Shr}	w_{Shr} (%)	ε_{Sw}	w_{Sw} (%)	ε_{Shr}	w_{Shr} (%)
P=0	0.1035	30	-0.1015	7.35	0.1055	24.69	-0.102	7.03	0.1065	23.78	-0.1021	7
P=1	0.0807	27.95	-0.101	7.1	0.0805	22	-0.1021	7	0.0805	20.71	-0.1024	7
P=2	0.07	25.05	-0.1051	7	0.073	20.06	-0.1057	6.95	0.072	18.2	-0.1064	6.95
P=3	0.0635	22.6	-0.1034	6.98	0.0645	17.83	-0.1058	6.96	0.066	16.4	-0.1065	6.95

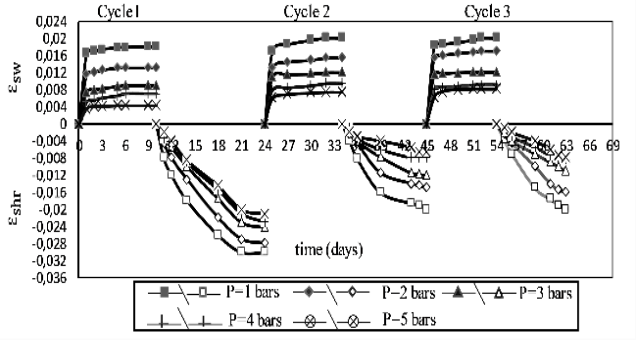

Figure 16. Cyclic variation of ESw and EShr relevant to Mustafaev [19].

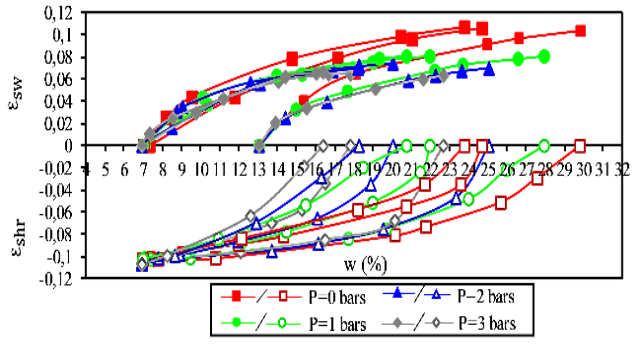

Figure 17. Cyclic evolution of the swelling-shrinkage potentials in terms of w (%).

In order to address the evolution of $\mathcal{E}_{Sw}$ and $\mathcal{E}_{Shr}$ with the cyclic effect of the maximal magnitude reached for $w(\%)$ within cyclic analyses that are recapitulated in Table (8), Figure (18a) shows distinguishable plots for cycle 1, while both cycles 2 and 3 are declining within a relatively narrow band; hence, the water content pertaining to cycles 2 and 3 is noticeably dropping with the rise of P compared to cycle 1. This is due to the high rate of water evacuation relevant to the increased pore water pressure caused by the reduced void spaces within the sample; in which, it contributes to restoring the effective stress on soil. Figure (18b) shows that $\mathcal{E}_{Sw}$ rises in value with the rise of w. Subsequently, the effect of load on the maximal value of w relevant to each cycle is employed to investigate the effect of P on the resulting $\mathcal{E}_{Sw}$ and $\mathcal{E}_{Sh}$, as shown in Figure (19). This figure depicts the relationship between $\mathcal{E}_{Sw}$ and $\mathcal{E}_{Shr}$ to understand the soil interaction under mechanical loadings. A higher ratio of $\mathcal{E}_{Sw}/\mathcal{E}_{Shr}$ indicates that the swelling is dominating under lower loads, while a lower value implies that the shrinkage is dominating under more significant loadings. This figure is crucial for the prediction of heave and settlement occurring to expansive soils under foundations.

4.3.3 Empirical equations for the swelling and shrinkage potentials in terms of t, w and P

On the basis of the above tests, four innovative equations are determined through various cycles to account for the time t and moisture content w under the effect of load P.

$$\varepsilon_{Sw}(t) = a_1 - b_1/t + c_1 \quad (7)$$

$$\varepsilon_{Shr}(t) = -a_1 + b_1/t - c_1 \quad (8)$$

$$\varepsilon_{Sw}(w) = a_2 - b_2/w + c_2 \quad (9)$$

$$\varepsilon_{Shr}(w) = -a_2 + b_2/w - c_2 \quad (10)$$

where, $a_{1,2}$, $b_{1,2}$, and $c_{1,2}$ are coefficients with regard to P, as computed in Tables (12 and 13). It follows, therefore, that $\mathcal{E}_{Sw}$ and $\mathcal{E}_{Shr}$ are defined by the innovative expressions that are applicable for this specific type of geographical location, as represented in Figures (20 and 21).

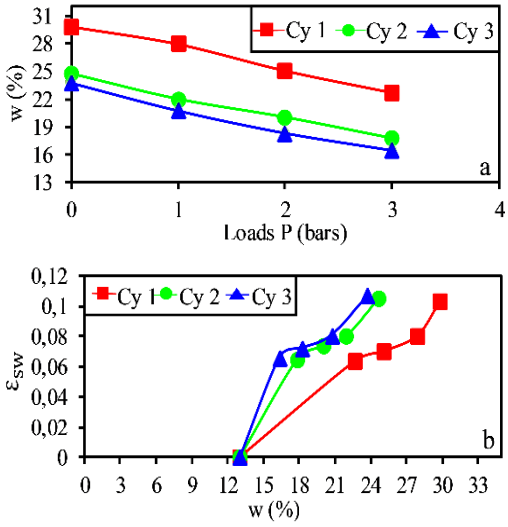

Figure 18. Effect of w on swelling cycles under a various range of P.

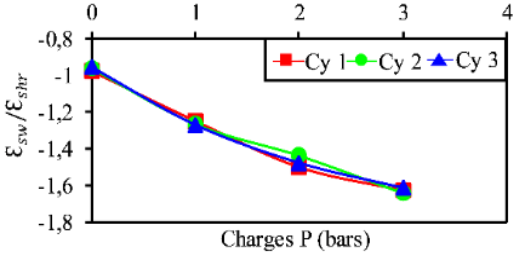

Figure 19. Cycles pertaining to εsw,/ εshr in terms of P.

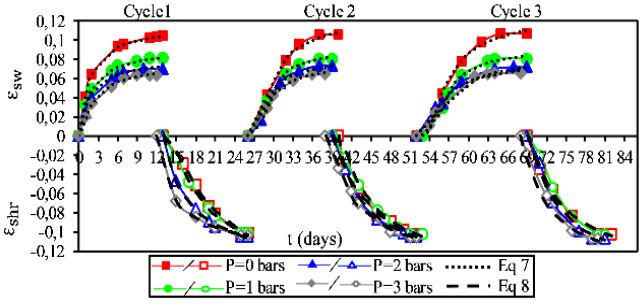

Figure 20. Application of the derived equations following the cyclic evolution of ESw-EShr in terms of t and P.

Table 12. Magnitude of the variables a1, b1 and c1 in terms of P in Eqs. (7 and 8).

Equations	Cycle 1	Cycle 2	Cycle 3
a_1	$\mathcal{E}_{Sw}$=0,055+0,11/(*P*+1,75) $\mathcal{E}_{Shr}$=-0,1+3,88/(*P*+14,01)	$\mathcal{E}_{Sw}$=0,062+0,07/(*P*+1,01) $\mathcal{E}_{Shr}$=-0,092+6,87/(*P*+27,3)	$\mathcal{E}_{Sw}$=0,078+0,027/(*P*+0,46) $\mathcal{E}_{Shr}$=0,146+0,001/(*P*-1,6)
b_1	$\mathcal{E}_{Sw}$=1,462+0,123/(*P*-0,364) $\mathcal{E}_{Shr}$=7,83+0,27/(*P*-0,17)	$\mathcal{E}_{Sw}$=-25,63-0,194/(*P*-0,38) $\mathcal{E}_{Shr}$=35,83-1,04/(*P*+0,29)	$\mathcal{E}_{Sw}$=-50,64+0,383/(*P*-1,15) $\mathcal{E}_{Shr}$=64,24-0.073/(*P*-2,07)
c_1	$\mathcal{E}_{Sw}$=0,156-0,005/(*P*-1,77) $\mathcal{E}_{Shr}$=-0,973+9,99/(*P*+4,12)	$\mathcal{E}_{Sw}$=0,132+0,064/(*P*+0,30) $\mathcal{E}_{Shr}$=-0,52+7,502/(*P*+4,63)	$\mathcal{E}_{Sw}$=0,331-0,065/(*P*-0,55) $\mathcal{E}_{Shr}$=-0,34+20,81/(*P*+19,44)

Table 13. Results of the variables a2, b2 and c2 in terms of P, relevant to Es. (9 and 10).

Equations	Cycle 1	Cycle 2	Cycle 3
a_2	$\mathcal{E}_{Sw}$=0,12+0,02/(*P*+0,73) $\mathcal{E}_{Shr}$=0,13+0,001/(*P*-1,41)	$\mathcal{E}_{Sw}$=0,074+0,062/(*P*+0,59) $\mathcal{E}_{Shr}$=0,131+0,06/(*P*-1,22)	$\mathcal{E}_{Sw}$=0,063+0,091/(*P*+1) $\mathcal{E}_{Shr}$=0,194-0,0011/(*P*-0,03)
b_2	$\mathcal{E}_{Sw}$=1,22-0,07/(*P*+0,24) $\mathcal{E}_{Shr}$=-0,6-0,04/(*P*+0,35)	$\mathcal{E}_{Sw}$=0,1+0,72/(*P*+0.4) $\mathcal{E}_{Shr}$=0,21-3,5/(*P*+1,16)	$\mathcal{E}_{Sw}$=0,03+0,811/(*P*+0,71) $\mathcal{E}_{Shr}$=-0,97-1,7/(*P*+0,38)
c_2	$\mathcal{E}_{Sw}$=-1,82-1,361/(*P*+0,31) $\mathcal{E}_{Shr}$=27,17+12,63/(*P*+1,72)	$\mathcal{E}_{Sw}$=-7+9,43/(*P*+0,94) $\mathcal{E}_{Shr}$=4,1+103,34/(*P*+2,7)	$\mathcal{E}_{Sw}$=-5,6+6,2/(*P*+0,94) $\mathcal{E}_{Shr}$=17,4+24,43/(*P*+0,8)

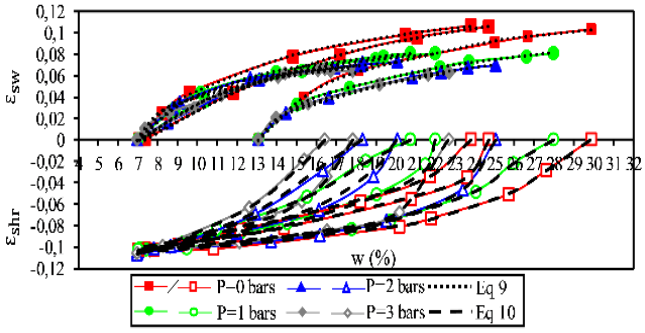

Figure 21. Application of current equations for the cyclic evolution of ℇSw-ℇShr in terms of w (%).

According to the approach of Mustafaev [19], Eqs. (11-16) are derived in terms of the initial water content relevant to the swelling-shrinkage in order to compute their respective potentials. Figure 22 (a and b) shows a comparison between current results relevant to *P*=0 that have been dressed with respect to Eqs. (7-10) with those of Mustafaev; a discernible parallelism between the studies is exhibited in a consistent manner following a similar constitutive law with caution regarding the environmental conditions between both regions is expressed by the slight difference between both studies

$$\varepsilon_{sw} = \alpha_H \, e^{t^{\beta_H}} \tag{11}$$

$$\varepsilon_{shr} = -\alpha_y \, e^{t^{\beta_y}} \tag{12}$$

$$\varepsilon_{sw} = 1 - e^{\alpha_h (W - W_H)} \tag{13}$$

$$\varepsilon_{shr} = 1 - e^{\alpha_y (W - W_{shr})} \tag{15}$$

$$\alpha_H = \frac{1}{W_{sw} - W_h} \ln \frac{1}{1 - \varepsilon_{sw}^k} \tag{16}$$

where, β_H and β_y are the parameters of nonlinear deformations relevant to swelling-shrinkage. ε_{sw}^k et ε_{shr}^k are derived in terms of the initial water content of soil relevant to swelling and shrinkage, respectively.

5. Conclusion

This paper addresses the study of various wetting-drying paths on specimens of an intact undisturbed soil pertaining to the Algerian region of N'Gaous that is located in the east of Batna province. The soil characteristics (P_s=695 kPa, P_c=750 kPa, I_p= 43.07% and w=13,06%) show a high rate of plasticity that implies a swelling tendency. The oedometric test has been modified in order to incorporate the thermal effect in the investigation of both swelling and shrinkage at a time.

It is noted from the obtained results that the cyclic alterations in wetting-drying paths significantly influence the potential of swelling and shrinkage coefficients, this essentially depends on the internal structure of the clay and fast absorption of water due to the suction force that determines the clay permeability. In agreement with previously published experimental data, the present results assert that the intensity of deformation caused by swelling-shrinkage strains and applied loads during wetting-drying paths influences the absorption character in the soil specimen. The swelling-shrinkage potentials increase significantly during the first cycles; the maximal value of the water content relevant to the swelling is attained at t=13 days, while that of shrinkage is at t=26 days. w_{Sw} is found to be following a decreasing tendency from its initial magnitude, while w_{Shr} is almost constant, independently of the loading. Furthermore, the vertical swelling of clays may take bigger amplitudes; as for the 1st cycle, the load P=0 bars resulted in $\mathcal{E}_{Sw}$= 10,35% and $\mathcal{E}_{Shr}$= -10.15%; while for the 3rd cycle $\mathcal{E}_{Sw}$ is found to be of 10,65% and $\mathcal{E}_{Shr}$ of -10.21%. A rise of 0 to 2,33% is obtained for the swelling relevant to 1st and 3rd cycles. P=3 bars results in $\mathcal{E}_{Sw}$= 6,35% and $\mathcal{E}_{Shr}$= -10,34%. It was noted that the swelling potential is dropping by 38.65% from P=0 to 3 bars (1st cycle); thus, the corresponding shrinkage was noticed to be improving by 1.87%. In contrast, the plots pertaining to cycles 2 and 3 fall almost in a tight band for P=2 and 3 bars. It was noted that the rise in the number of wetting cycles slightly increases the deformation, whereas for the shrinkage, the effect is negligible leaning towards constant values. This is expressed by the dependency of the swelling-shrinkage magnitude on the initial water content. The ratio $\mathcal{E}_{Sw}/\mathcal{E}_{Shr}$ was investigated to predict the heave and settlement under loading; it was found that the increase in the swelling strains is controlled by the magnitude of water content. The latter is amplified by 20,90% for the first cycle compared to the 2nd under P=0; hence, it is only of 3,83% between the 2nd and 3d cycles. In direct correlation with the proliferation of the applied loads, the rate of water infiltration decreases for the first cycle under P=3 Bars by 27,16% compared to the 2nd; and 8.65% from cycle 2 to 3.

The actual results induce a deformation that is more important than that estimated without the thermal factor implementation. Given that the classical methods have proven their inaccuracy in the estimation of the soil deformations, this calls for the necessity of replicating environmental conditions in all types of geotechnical investigations in order to preserve human and economic losses.

It should be emphasized that the current results are only valid for the considered type of clay and under the stated testing conditions, as the thermal fluctuations during seasonal changes may influence significantly the rate of deformations within the soil in the long-term. Nevertheless, a simple objective may lighten other complex case studies in order to account for effective mitigation strategies for reducing the impact of expansive and contractive soils on the infrastructure, as well

as contributing to the enhancement of the generalizability of results in broader geographical regions.

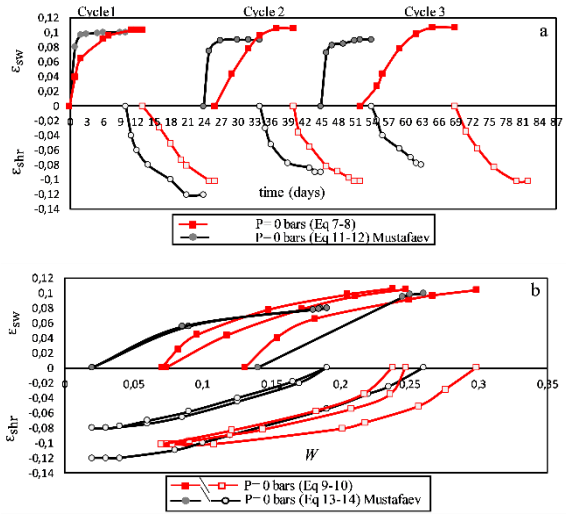

Figure 22. Correlation between the equations derived from the current study and those of Mustafaev [19].

Disclosure statement

No potential conflict of interest was reported by the authors.

References

[1] Medjnoun, A., Khiatine, M. & Bahar, R. (2014). Caractérisation minéralogique et géotechnique des argiles marneuses gonflantes de la région de Médéa, Algérie. Bulletin of Engineering Geology and the Environment, Springer, 73 (4).

[2] Mebarki, M., Kareche, T., Derfouf, F. E. M., Taibi, S. & Aboubekr, N. (2019). Hydromechanical behavior of a natural swelling soil of Boumagueur region (east of Algeria). Geomechanics and Engineering, 17, 69-79. https://doi.org/10.12989/GAE.2019.17.1.069

[3] Bourokba Mrabent, S.A., Hachichi, A., Souli, H., Taibi, S. & Fleureau, J. M. (2017). Effect of lime on some physical parameters of a natural expansive clay from Algeria. European Journal of Environmental and Civil Engineering, Taylor & Francis. 21, 108-25.

[4] Athmania, D., Benaissa, A., Hammadi, A. & Bouassida, M. (2010). Clay and marl formation susceptibility in Mila Province, Algeria. Geotechnical and Geological Engineering, Springer. 28, 805-13.

[5] Medjnoun, A. et Bahar, R. (2016) Shrinking–swelling of clay under the effect of hydric cycles. Innovative Infrastructure Solutions, Springer. 1, 1-8.

[6] Smaida, A., Mekerta, B. & Gueddouda, M. K. (2021). Physico-mechanical stabilization of a high swelling clay. Construction and Building Materials, Elsevier. 289, 123197.

[7] Khennouf, A., Baheddi, M. (2020). Heave analysis of shallow foundations founded in swelling clayey soil at N'Gaous city in Algeria. Studia Geotechnica et Mechanica, 42, 210-21. https://doi.org/10.2478/sgem-2019-0051

[8] Derriche, Z., Cheikh-Lounis, G. (2004). Geotechnical characteristics of the Plaisancian marls of Algiers. Bulletin of Engineering Geology and the Environment, Springer. 63, 367-78.

[9] Rathore, P., Tiwari, S. K. (2023). Soil Stabilization using Ceramic Waste: an Experimental Study. Journal of Mining and Environment. 14 (1), 47-65.

[10] Rao, S. M., Reddy, B. V. V. & Muttharam, M. (2001). The impact of cyclic wetting and drying on the swelling behaviour of stabilized expansive soils. Engineering geology, Elsevier. 60, 223-33.

[11] Nabil, M., Mustapha, A. & Rios, S. (2020). Impact of wetting—drying cycles on the mechanical properties of lime-stabilized soils. International Journal of Pavement Research and Technology, 13, 83-92. https://doi.org/10.1007/s42947-019-0088-y

[12] Dakshanamurthy, V., Raman, V. (1973). A simple method of identifying an expansive soil. Soils and foundations. The Japanese Geotechnical Society, 13, 97-104.

[13] Djedid, A., Bekkouche, A. & Mamoune, S. M. (2001). Identification and prediction of the swelling behavior of some soils from the Tlemcen region of Algeria. Bulletin des laboratoires des ponts et chaussées, 233, 69-77.

[14] Huang, C., Wang, X., Zhou, H. & Liang, Y. (2019). Factors affecting the swelling-compression characteristics of clays in Yichang, China. Adv. Civ Eng, 1. https://doi.org/10.1155/2019/6568208

[15] Estabragh, A. R., Parsaei, B. & Javadi, A. A. (2015). Laboratory investigation of the effect of cyclic wetting and drying on the behaviour of an expansive soil. Soils and foundations, Elsevier. 55, 304-14.

[16] Zeng, Z., Kong, L., Wang, M. & Sayem, H. M. (2018). Assessment of engineering behaviour of an intensely weathered swelling mudstone under full range of seasonal variation and the relationships among measured parameters. Canadian Geotechnical Journal. NRC Research Press. 55, 1837-49.

[17] Soltani, A., Taheri, A., Khatibi, M. & Estabragh, A. R. (2017). Swelling potential of a stabilized expansive soil: a comparative experimental study. Geotechnical and Geological Engineering, Springer. 35, 1717-44.

[18] Abbas, M. F., Shaker, A. A. & Al-Shamrani, M. A. (2023). Hydraulic and volume change behaviors of compacted highly expansive soil under cyclic wetting and drying. Journal of Rock Mechanics and Geotechnical Engineering, Elsevier. 15, 486-99.

[19] Mustafaev, A. A. (1989). Фундаменты на просадочных и набухающих грунтах. М.: Высшая школа. 588.

[20] Zemenu, G., Martine, A. & Roger, C. (2009). Analysis of the behaviour of a natural expansive soil under cyclic drying and wetting. Bulletin of Engineering Geology and the Environment, 68, 421-36. https://doi.org/10.1007/s10064-009-0203-4

[21] Onyelowe, K. C., Aneke, F. I., Onyia, M. E., Ebid, A. M. & Usungedo, T. (2023). AI (ANN, GP, and EPR)-based predictive models of bulk density, linear-volumetric shrinkage & desiccation cracking of HSDA-treated black cotton soil for sustainable subgrade. Geomechanics and Geoengineering, Taylor & Francis.

[22] Onyelowe, K. C., Ebid, A. M., Onyia, M. E. & Amanamba, E. C. (2022). Estimating the swelling potential of non-carbon–based binder (NCBB)-treated clayey soil for sustainable green subgrade using AI (GP, ANN and EPR) techniques. International Journal of Low-Carbon Technologies, 17, 807-15. https://doi.org/10.1093/ijlct/ctac058

[23] Dao, H. M., Nguyen, A. T. T., Do, T. M. & Do, T. M. (2020). Effect of wetting-drying cycles on surface cracking and swell-shrink behavior of expansive soil modified with ionic soil stabilizer. Journal of Mining and Earth Sciences, 61, 1-13.

[24] Aneke, F. I., Onyelowe, K. C. & Ebid, A. M. (2024). AI-Based Estimation of Swelling Stress for Soils in South Africa. Transportation Infrastructure Geotechnology, 11, 1049-72.

https://doi.org/10.1007/s40515-023-00311-4

[25] Onyelowe, K. C., Ebid, A. M., Nwobia, L. I. & al. (2022). Shrinkage Limit Multi-AI-Based Predictive Models for Sustainable Utilization of Activated Rice Husk Ash for Treating Expansive Pavement Subgrade. Transp. Infrastruct. Geotech, 9, 835–853. https://doi.org/10.1007/s40515-021-00199-y

[26] Aneke, F. I., Onyelowe, K. C., Ebid, A. M. & al. (2022). Predictive models of swelling stress—a comparative study between BP- and GRG-ANN. Arab J Geosci 15, 1438. https://doi.org/10.1007/s12517-022-10706-1

[27] ASTM D4546-08. (2008). Standard Test Method for One-Dimensional Swell or Settlement Potential of Cohesive Soil. ASTM International West Conshohocken, PA.

[28] ASTM D4546-03. (2003) Standard Test Methods For One-Dimensional Swell Or Settlement Potential Of Cohesive Soils. Annual Book of ASTM Standards, ASTM International West Conshohocken, PA, USA. 04, 992-1001.

[29] ASTM, A. (2003) Standard test methods for one-dimensional swell or settlement potential of cohesive soils. ASTM International West Conshohocken, PA.

[30] AFNOR. (1995) NF P94-091 Détermination des déformations par chargement de plusieurs éprouvettes.